

Unsupervised Blood Vessel Segmentation of Fundus Images Based on Region Features and Hierarchical Growth Algorithm

Zhun Fan, *Senior Member, IEEE*, Jiewei Lu, Wenji Li

Abstract—Automated blood vessel segmentation plays an important role in the diagnosis and treatment of various cardiovascular and ophthalmologic diseases. In this paper, a novel unsupervised segmentation algorithm is proposed to extract blood vessels from fundus images. At first, an enhanced vessel image is generated by morphological reconstruction, and then divided into three parts: preliminary vessel regions, background regions and undetermined regions. Secondly, a list of region features of blood vessels are defined and used to remove the noise regions in preliminary vessel regions and extract the skeletons of blood vessels. An intermediate vessel image is obtained by combining the denoised preliminary vessel regions with vessel skeletons. After that, a novel hierarchical growth algorithm, namely HGA, is proposed to label each pixel in undetermined regions as vessel or non-vessel in an incremental way, which takes the advantage of color and spatial information from the intermediate vessel image and the background regions. Finally, postprocessing is performed to remove the non-vessel regions. The proposed algorithm has low computational complexity and outperforms many other state-of-art supervised and unsupervised methods in terms of accuracy. It achieves a vessel segmentation accuracy of 96.0%, 95.7% and 95.1% in an average time of 10.72s, 15.74s and 50.71s on images from three publicly available fundus image datasets DRIVE, STARE, and CHASE_DB1, respectively.

Index Terms—Vessel segmentation, fundus images, region features, vessel skeletons, hierarchical growth algorithm.

I. INTRODUCTION

RETINAL blood vessels generally show a coarse to fine centrifugal distribution and appear as a wire mesh-like structure or tree-like structure. Their morphological features, such as length, width and branching, play an important role in diagnosis, screening, early detection and treatment of various cardiovascular and ophthalmologic diseases such as stroke, vein occlusions, diabetes and arteriosclerosis [1]. The analysis of morphological features of retinal blood vessels can facilitate a timely detection and treatment of a disease when it is still in its early stage. Moreover, the analysis of retinal blood vessels can assist in evaluation of retinal image registration [2], the relationship between vessel tortuosity and hypertensive retinopathy [3], retinopathy of prematurity [4], arteriolar narrowing [5], mosaic synthesis [6], biometric identification [7], foveal avascular region detection [8] and computer-assisted laser surgery [1]. Since cardiovascular and ophthalmologic diseases have a serious impact on human's life, the analysis of retinal blood vessels becomes more and more important,

and is of great significance in many clinical applications to reveal important information of systemic diseases and support diagnosis and treatment. As a result, the requirement of vessel analysis system grows rapidly in which the segmentation of retinal blood vessels is the first and one of the most crucial steps.

The segmentation of retinal blood vessels has been a heavily researched area in recent years [9]. Broadly speaking, existing algorithms can be divided into supervised and unsupervised methods. In supervised methods, a number of different features are extracted from fundus images, and applied to train the effective classifiers with the purpose of extracting retinal blood vessels. In [10], Staal *et al.* extracts 27 features for each image pixel with ridge profiles, and performs feature selection by using sequential forward selection method to pick those pixels that result in better segmentation performance by a K-Nearest Neighbor (KNN) classifier. Soares *et al.* [11] introduces a feature-based Bayesian classifier with Gaussian mixtures for vessel segmentation, which uses the intensity information and Gabor wavelet transform responses to build a 7-D feature vector for each pixel. In [12], Lupascu *et al.* utilizes an AdaBoost classifier and a 41-D feature vector which includes information on the local intensity structure, spatial properties, and geometry at multiple scales. Marin *et al.* [13] constructs a 7-D vector composed of gray-level and moment invariants-based features, and then trains a neural network (NN) for pixel classification. Roychowdhury *et al.* [14] extracts the major vessel from the fundus images and uses a Gaussian Mixture Model classifier for vessel segmentation with a set of 8 features, which are extracted based on pixel neighborhood and first and second-order gradient images. In [15], Liskowski employs a deep neural network to extract vessel pixels from fundus images. In unsupervised methods, the researchers try to find inherent properties of retinal blood vessels that can be applied to extract vessel pixels from fundus images. The unsupervised methods can be further divided into multiscale approaches, matched filtering, vessel tracking, mathematical morphology and model based methods [9]. The multiscale approach introduced by [16] develops a vessel enhancement filter with the analysis of multiscale second order local structure of an image (Hessian), and obtains a vesselness measure by using the eigenvalues of the Hessian. The matched filtering method described by [17] employs different threshold probes to extract blood vessels from matched filter response images. In [18], the methodology based on vessel tracking applies a wave propagation and traceback mechanism to label each pixel

Zhun Fan, Jiewei Lu and Wenji Li are with the Department of Electrical Information Engineering, Shantou University, Shantou, Guangdong (email: fzfzfan, 12jwlu1, liwj@stu.edu.cn)



Fig. 1: The process of the proposed algorithm

the likelihood of belonging to vessels in angiography images. The mathematical morphology with the extraction of vessel centerlines [19] is also developed to find the morphological characteristics of retinal blood vessels. Model based methods generally use geometric deformable models [20], parametric deformable models [21], vessel profile models [22] and active contour models [23] for blood vessel segmentation.

Most unsupervised methods do not make full use of the determined information (determined vessel information and background information) to estimate the undetermined regions. In order to take full advantage of the determined information, a novel unsupervised algorithm is proposed for blood vessel segmentation. The proposed algorithm divides the image into determined regions (vessel regions and background regions) and undetermined regions, and extracts vessel pixels in the undetermined regions by using HGA. Moreover, the proposed algorithm extracts the vessel regions and background regions first, which leads to a significant reduction on the load of pixel classification of the fundus image. The proposed method is evaluated on three public available datasets DRIVE, STARE, and CHASE_DB1, which have been widely used by other researchers to develop their own algorithms. The vessel segmentation performance demonstrates the effectiveness of the proposed vessel segmentation algorithm.

The rest of this paper is structured as follows: Section II details the proposed methodology. Section III introduces the public available datasets and the commonly used evaluation metrics. Section IV presents the experimental results. In Section V, the discussion and conclusion are given.

II. METHODOLOGY

The proposed algorithm is inspired by image matting [24]–[26], which refers to the problem of accurately extracting the foreground from an image. Image matting is often implemented with a user-specified trimap [24], which separates the image into three parts: a foreground image, a background image and an undetermined image. The matting methods try to estimate the undetermined image with the foreground image and the background image.

Inspired by the basic idea of image matting, the proposed vessel segmentation algorithm is performed in three stages. In the first stage, an enhanced vessel image is generated by morphological reconstruction, and then divided into three parts: preliminary vessel regions, background regions and undetermined regions. Then a list of region features of blood vessels are defined and used to remove the noise regions in the preliminary vessel regions. The region features are also applied to extract vessel skeletons from another enhanced vessel image generated by the isotropic undecimated wavelet transform [27]. An intermediate vessel image is obtained by combing the denoised preliminary vessel regions with the vessel skeletons.

TABLE I: DEFINITIONS OF IMAGE NOTATIONS

Notations	Meanings
I_{e1}	The first enhanced vessel image
B	Background regions
U	Undetermined region
V_1	Preliminary vessel regions
V_2	Denoised preliminary vessel regions
I_{e2}	The second enhanced vessel image
S	Vessel skeletons
V_3	An intermediate vessel image
V	The estimated vessel image

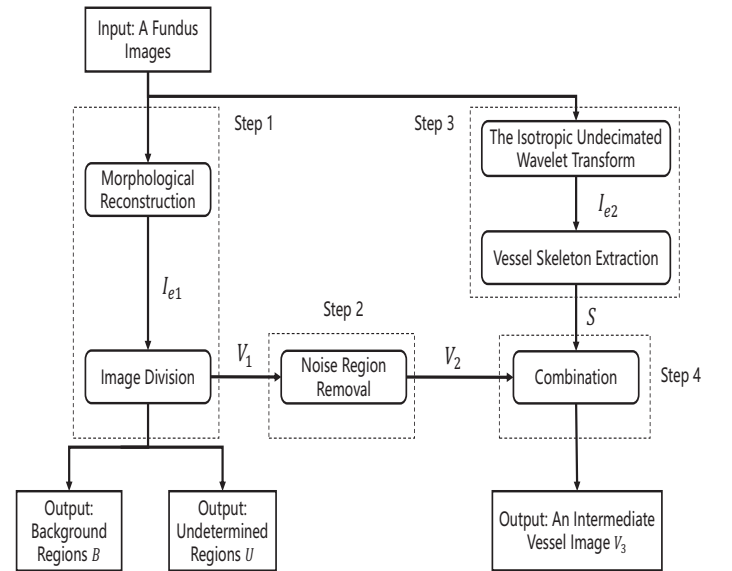


Fig. 2: The framework of stage 1

In the second stage, a novel hierarchical growth algorithm (HGA) is proposed to classify all undetermined pixels in the undetermined image. HGA labels each pixel in the undetermined regions as vessel or non-vessel in an incremental way by using color and spatial information from the intermediate vessel image and the background regions. In the last stage, postprocessing is applied to remove the non-vessel regions. The process of the proposed algorithm is shown in Fig.1. The image notations and their definitions used in the proposed algorithm are shown in Table I.

A. Stage 1: The Preliminary and Intermediate Region Segmentation

In stage 1, the main goal is to obtain undetermined regions, determined vessel regions and background regions. This stage consists of the following four steps: 1) image division, 2) noise region removal, 3) vessel skeleton extraction and 4) combination. The framework of stage 1 is shown in Fig.2. The

TABLE II: DEFINITIONS OF MASTER PARAMETERS

Master Parameters	Meaning
$th1$	The upper threshold used to segment the image
e_1	The upper value of <i>Extensibility</i>
e_2	The lower value of <i>Extensibility</i>
r	The threshold of <i>VRatio</i>
s	The threshold of <i>Solidity</i>
f_i	The internal factor. f_i is calculated as $d \times \frac{\max(h,w)}{\min(h,w)}$, $d = 21$ is approximately the diameter of the biggest vessels in fundus images [28], h and w are the height and width of the fundus image.

TABLE III: DEFINITIONS OF DERIVATIVE PARAMETERS

Derivative Parameters	Meaning
$th2$	The lower threshold used to segment the image. $th2$ is calculated as $th1 - 0.15$.
a_1	The first threshold of <i>Area</i> a_1 is calculated as $f_i \times 2$.
a_2	The second threshold of <i>Area</i> a_2 is calculated as $f_i \times 8$.
a_3	The third threshold of <i>Area</i> a_3 is calculated as $f_i \times 2.5$.
a_4	The fourth threshold of <i>Area</i> a_4 is calculated as $f_i \times 35$.

definitions of master parameters used in stage 1 are shown in Table II, and the definitions of derivative parameters used in stage 1 are shown in Table III. The experimental setting and analysis of master parameters will be presented in Section III.

1) *Image Division*: Before performing image division, since color fundus images often show poor contrast between vessels and background [13], morphological reconstruction is applied to enhance the contrast and generate images more suitable for image division.

For each fundus image, the green channel fg is extracted at first [29]. Then fg scaled in $[0,1]$ is processed by an adaptive median filter with the purpose of removing the salt-and-pepper noise. The median filter starts at size 3-by-3 and iterates up to size 7-by-7. Next, the complement image fg_c of the processed green channel image is subjected to contrast enhancement by morphological reconstruction [28]:

$$I_{th}^\theta = fg_c - (fg_c \circ S_e^\theta) \quad (1)$$

The morphological top-hat transformation is given in Equation (1), where I_{th}^θ represents the top-hat transformed image, S_e is a structuring element for morphological opening \circ , and θ specifies the angle (in degrees) of the structuring element. The structuring element is of 1-pixel width and 21-pixels length, which approximately fits the diameter of the biggest vessels in the fundus images [28]. Since the morphological top-hat transformation transformation given in Equation (1) can only brighten blood vessels in one direction, the sum of top-hat transformation I_{th}^θ along each direction is performed in order to enhance the whole vessel image.

$$I_{e1} = \sum_{\theta \in A} I_{th}^\theta \quad (2)$$

The sum of top-hat transformation is depicted in Equation (2), where I_{e1} represents the enhanced vessel image, "A" is

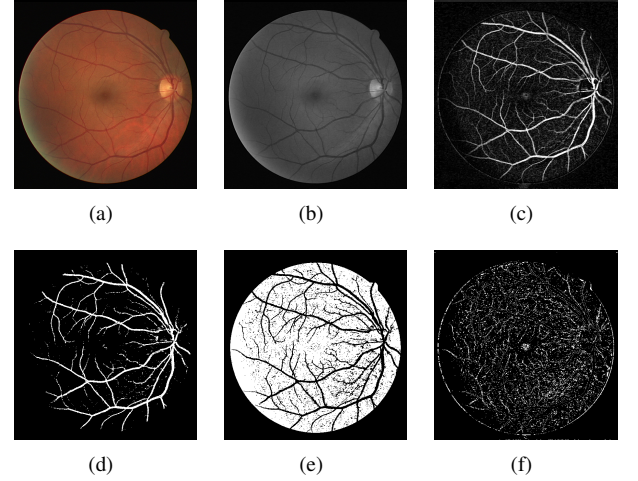


Fig. 3: Image division of an image from DRIVE dataset. (a) The fundus image (b) The green channel of the fundus image fg . (c) The enhanced vessel image I_{e1} . (d) Preliminary vessel regions V_1 . (e) Background regions B . (f) Undetermined regions U .

the set of angles of the structuring element and defined as $\{x | 0 < x < \pi \ \& \ x \bmod (\pi/12) = 0\}$.

For each enhanced vessel image I_{e1} , in order to make full use of the vessel information and background information, I_{e1} is divided into three parts: preliminary vessel regions (V_1), background regions (B) and undetermined regions (U) by two fixed thresholds $th1$ and $th2$.

$$I_{e1} = \begin{cases} B & \text{if } 0 < I_{e1} < th2 \\ U & \text{if } th2 \leq I_{e1} < th1 \\ V_1 & \text{if } th1 \leq I_{e1} \end{cases} \quad (3)$$

An example of image division using an image from DRIVE dataset [10] is shown in Fig.3.

2) *Noise Region Removal*: A list of region features of blood vessels are defined and used to remove the noise regions in preliminary vessel regions. These region features characterize the morphological properties of blood vessels [9] and are suitable to be applied for blood vessel segmentation. The definition of region features are given as follows [30], [31].

- **Area** is the actual number of pixels in each connected region.
- **Bounding Box** (Fig.4) specifies the smallest rectangle containing the region.
- **Extensibility** is the ratio of pixels in the connected region to pixels in the total bounding box.
- **VRatio** is the ratio of width and length of the bounding box.
- **Convex Hull** (Fig.4) specifies the smallest convex polygon that can contain the connected region.
- **ConvexArea** specifies the number of pixels in convex hull.
- **Solidity** is the ratio of pixels in the connected region to pixels in the total convex hull.

For preliminary vessel regions, the regions with $a_1 \leq Area_{V1} \leq a_2$ are extracted first (V_1^*). Then connected regions in V_1^* with $Extensibility \leq e1$ && $VRatio \leq r$ && $Solidity \geq s$ are abandoned, resulting in the denoised preliminary vessel regions V_2 .

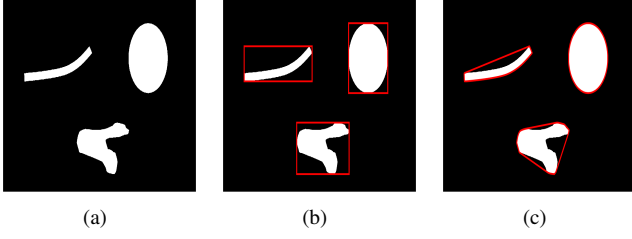


Fig. 4: An example to illustrate the bounding box and convex hull. (a)The exemplary image. (b)The image for the illustration of bounding box. The red boxes are the bounding boxes. (c)The image for the illustration of convex hull. The red polygons are the convex hulls.

3) *Vessel Skeleton Extraction*: The basic idea of the proposed algorithm is making use of the determined information (determined vessel information and background information) to estimate the undetermined regions. After applying image division and noise region removal, the determined vessel information and background information can be obtained from V_2 and B . In order to provide enough vessel information, vessel skeleton extraction is performed. The analysis of vessel skeleton extraction will be given in Section IV.

Since the enhanced vessel image I_{e1} could not reflect the connected properties of blood vessels completely [32], it is difficult to extract sufficient available vessel skeletons from I_{e1} alone. Hence, the isotropic undecimated wavelet transform [27] is employed to generate another vessel enhanced image, which is more suitable for vessel skeleton extraction.

The isotropic undecimated wavelet transform (IUWT) is a powerful wavelet transform, which has been applied for vessel segmentation and shows good performance. Applied to a signal $c_0 = fg$, scaling coefficients are computed by convolution with a filter $h^{\uparrow j}$

$$c_{j+1} = c_j * h^{\uparrow j} \quad (4)$$

where $h_0 = [1, 4, 6, 4, 1]/16$ is derived from the cubic B-spline, $h^{\uparrow j}$ is the upsampled filter obtained by inserting $2^j - 1$ zeros between each pair of adjacent coefficients of h_0 . Wavelet coefficients are the difference between two adjacent sets of scaling coefficients, i.e.,

$$w_{j+1} = c_j - c_{j+1} \quad (5)$$

Reconstruction of the original signal from all wavelet coefficients and the final set of scaling coefficients is straightforward, and requires only addition. The enhanced vessel image after IUWT is depicted as follows:

$$I_{e2} = c_n + \sum_{j=2}^3 w_j \quad (6)$$

The wavelet scales:2-3 in Equation (6) are selected according to [27].

After performing the isotropic undecimated wavelet transform, a binary image T is obtained by global thresholding the enhanced vessel image I_{e2} for pixels greater than 0.003.

$$T = \begin{cases} 1 & I_{e2} > 0.003 \\ 0 & I_{e2} \leq 0.003 \end{cases} \quad (7)$$

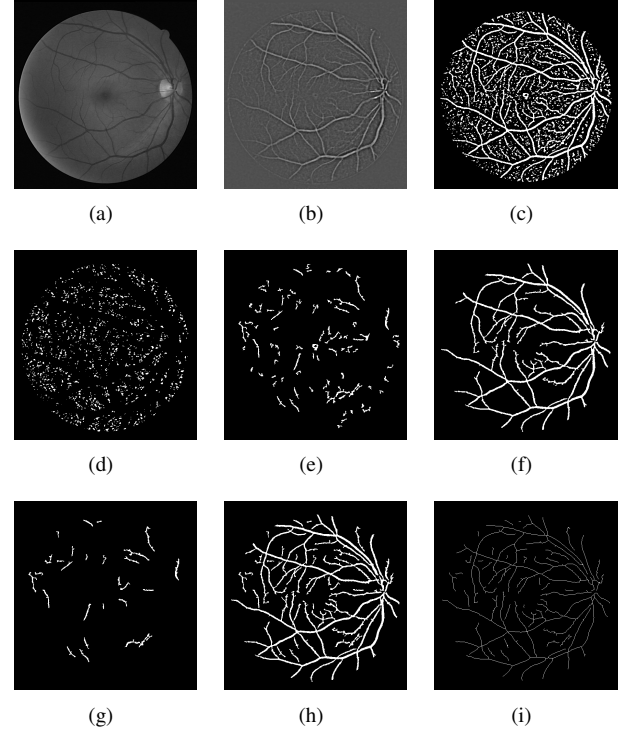


Fig. 5: Vessel skeleton extraction of an image from DRIVE dataset. (a) The green channel of the fundus image fg . (b)The vessel enhanced image I_{e2} . (c) The binary image T . (d) Background regions $T1$. (e) Candidate regions $T2$. (f) Vessel regions $T3$. (g) $T4$: The preserved regions in $T2$. (h) The combined regions of $T3$ and $T4$ (h) The vessel skeletons S .

For image T , the connected regions are divided into three parts: background regions($T1$), candidate regions($T2$) and vessel regions($T3$) according to the *Area* feature of each connected region:

$$T = \begin{cases} T1 & \text{if } 0 < Area_T < a_3 \\ T2 & \text{if } a_3 \leq Area_T \leq a_4 \\ T3 & \text{if } a_4 < Area_T \end{cases} \quad (8)$$

The regions in $T3$ are preserved while the regions in $T1$ are abandoned. Then the regions in $T2$ with *Extensibility* $> e_2$ && *VRatio* $\leq r$ are preserved as $T4$. Finally skeleton extraction [33] is performed on the combined regions of $T3$ and $T4$ in order to obtain the skeleton of blood vessels S . Fig.5 gives an example of vessel skeleton extraction using the same image from DRIVE dataset.

4) *Combination*: After performing noise region removal and vessel skeleton extraction, an intermediate vessel image V_3 is obtained by combing the denoised preliminary vessel regions V_2 with vessel skeletons S .

B. Stage 2: Hierarchical Growth Algorithm (HGA)

In order to classify the pixels in U , HGA is proposed to label each undetermined pixel as vessel or non-vessel in an incremental way. HGA is inspired by the non-dominated sorting approach [34], [35]. The non-dominated sorting approach

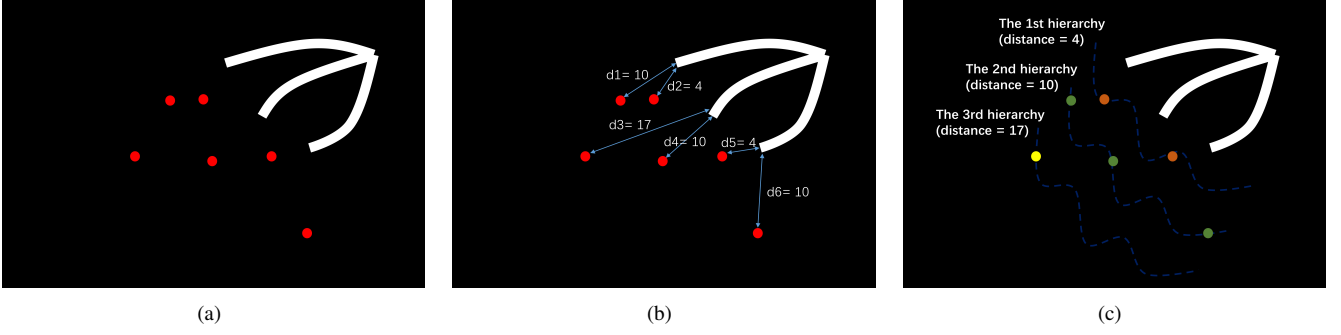


Fig. 6: A simple example to illustrate the process of initialization. (a) An exemplary image (white pixels represent vessel pixels, red pixels represent undetermined pixels). (b) Calculating the closest distance for each undetermined pixel (d_i means the closest distance for the i th undetermined pixel). (c) Separating undetermined pixels into different hierarchies.

plays an important role in multiobjective evolutionary algorithms (MOEAs), and can effectively separate the overall non-dominated set of solutions into different ranks [36] (Fig.7).

HGA consists of two main steps.

Step 1 *Initialization*: Separate pixels in U into different hierarchies.

Step 2 *Hierarchy Update*: Assign new labels (V or B) to pixels in each hierarchy.

The pseudocode of HGA is given in Algorithm 1.

Algorithm 1: Hierarchical Growth Algorithm

Input:

- 1) V_3 : an intermediate vessel image;
- 2) B : background regions;
- 3) U : undetermined regions;

Output: The estimated vessel image V

Step 1: Initialization:

- a) For $i = 1, \dots, n_U$, set $D(i) = d_i$, where n_U is the number of undetermined pixels in U , d_i is the distance between the i th undetermined pixel and the closest vessel pixel in V , D is the set of d_i .
- b) Sort the undetermined pixels in U in an ascending order according to the distances D , cluster the pixels with the same distance into one hierarchy, divide the pixels into m hierarchies and denote them as an hierarchical order set: $H = \{H_1, H_2, \dots, H_m\}$, $H_j = \{u_i^j | i \in 1, 2, \dots, n_i\}$, where n_i is the number of undetermined pixels in the j th hierarchy H_j .

Step 2: Hierarchy Update

For $j = 1, \dots, m$, do

For $i = 1, \dots, n_i$, do

- a) Compute the correlations (Defined in Equation (11)) between u_i^j and its neighboring labeled pixels (vessel pixels and background pixels) included in a 9×9 grid.
- b) Choose the labeled pixel with the closest correlation, and assign its label (V or B) to u_i^j .

end for

end for

Initialization: In the initialization stage, for the i th undetermined pixel in U , its distances with all vessel pixels in V

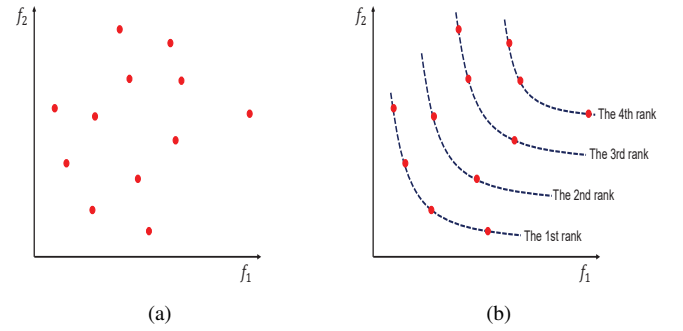


Fig. 7: The effect of non-dominated sorting. f_1 and f_2 are the objectives. Red points represent the solution individuals.

are calculated first. Then the closest distance is chosen for the i th undetermined pixel. After that, undetermined pixels are separated into different hierarchies according to the closest distances. The undetermined pixels reside in low hierarchy means that they are close to blood vessels; The undetermined pixels stay in high hierarchy means that they are far away from blood vessels. A simple example to illustrate the process of initialization is shown in Fig.6.

Correlation Function: In step 2 of the algorithm, given an undetermined pixel u_i^j and its neighboring labeled pixel k_l^j , a color cost function ξ_c is defined to describe the fitness of u_i^j and k_l^j first:

$$\xi_c(u_i^j, k_l^j) = \|c_{u_i^j} - c_{k_l^j}\| \quad (9)$$

where $c_{u_i^j}$ and $c_{k_l^j}$ are intensity level of u_i^j and k_l^j in I_{e1} . A spatial cost function ξ_s is further defined:

$$\xi_s(u_i^j, k_l^j) = \frac{\|x_{u_i^j} - x_{k_l^j}\| - x_{min}}{x_{max} - x_{min}} \quad (10)$$

where $x_{u_i^j}$ and $x_{k_l^j}$ are the spatial coordinates of u_i^j and k_l^j . The terms $x_{max} = \max_j \|x_{u_i^j} - x_{k_l^j}\|$ and $x_{min} = \min_j \|x_{u_i^j} - x_{k_l^j}\|$ are the maximum and minimum distance of the undetermined pixel u_i^j to the labeled pixel k_l^j . The normalization factors x_{min} and x_{max} ensure that ξ_s is independent from the absolute distance.

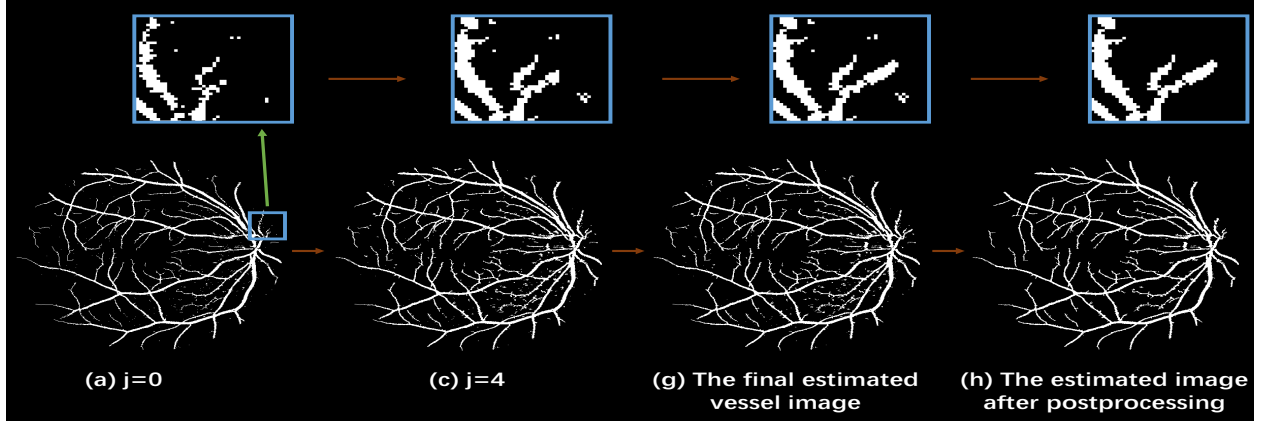


Fig. 8: Hierarchical growth algorithm and postprocessing. (a) Estimated vessel image in the hierarchy $j = 0$ (The intermediate vessel image V_3). (b) Estimated vessel image in the hierarchy $j = 4$. (c) The final estimated vessel image V . (d) The final estimated vessel image after postprocessing.

Our final correlation function ξ is a combination of the color fitness and the spatial distance:

$$\xi(u_i^j, k_l^j) = \xi_c(u_i^j, k_l^j) + \omega \xi_s(u_i^j, k_l^j) \quad (11)$$

where ω is a weight to trade off the color fitness and spatial distance. ω is set as 0.5 in our experiment. Intuitively, a small ξ indicates that the labeled pixel have a close correlation with the undetermined pixel and can well represent the undetermined pixel.

Hierarchy Update: After defining the correlation function, in each hierarchy, the correlations between each undetermined pixel and its neighboring labeled pixels (vessel pixels and background pixels) included in a 9×9 grid are computed. Then the label pixel with the closest correlation is chosen, and its label is assigned to the undetermined pixel (Fig.9).

After all undetermined pixels in one hierarchy are updated, they are used for the update of the next hierarchy. HGA iterates from the first hierarchy to the last one, which emulates a process that blood vessels grow from the intermediate vessel regions to the whole vessel regions.

An example of HGA is shown in Fig.8.

C. Stage 3: Postprocessing

Some non-vessel regions may still exist in the estimated vessel image V . To remove these non-vessel regions, the connected regions with $Area < a_4$ & $Extensibility > e_2$ & $VRatio < r$ in V are abandoned.

III. DATASETS AND EVALUATION METRICS

In this section, three publicly available datasets are introduced at first. These datasets have been widely used by a lot of researchers to develop their own vessel segmentation algorithms. Then the widely used evaluation metrics are presented, which are utilized in our experiment and for comparison with other state-of-art methods.

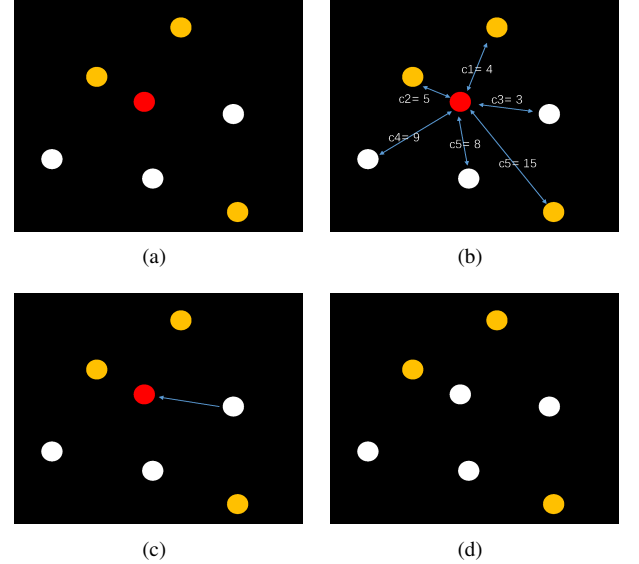


Fig. 9: An example for the illustration of assigning a label(V or B) to an undetermined pixel. (a) An exemplary image (white pixels represent vessel pixels, yellow pixels represent background pixels, red pixels represent undetermined pixels). (2) Calculating the correlation functions between a undetermined pixel and its neighboring labeled pixels (vessel pixels and background pixels) (c_i means the correlation between the undetermined pixel and the i th labeled pixel). (3) Assigning a label(V or B) to the undetermined pixel. (4) The resultant image.

A. Datasets

DRIVE¹ [10] consists of 40 fundus images obtained from a screening program in the Netherlands. These images are captured by a Canon CR5 non-mydratic 3-CCD camera at 45° field of view (FOV), and the size of each image is of 584×565 pixels. The DRIVE dataset is divided into two sets: a training set (DRIVE Training) and a test set (DRIVE Test) each containing 20 fundus images. The test set is annotated by two independent human observers, resulting in a set X and

¹<http://www.isi.uu.nl/Research/Databases/DRIVE/>

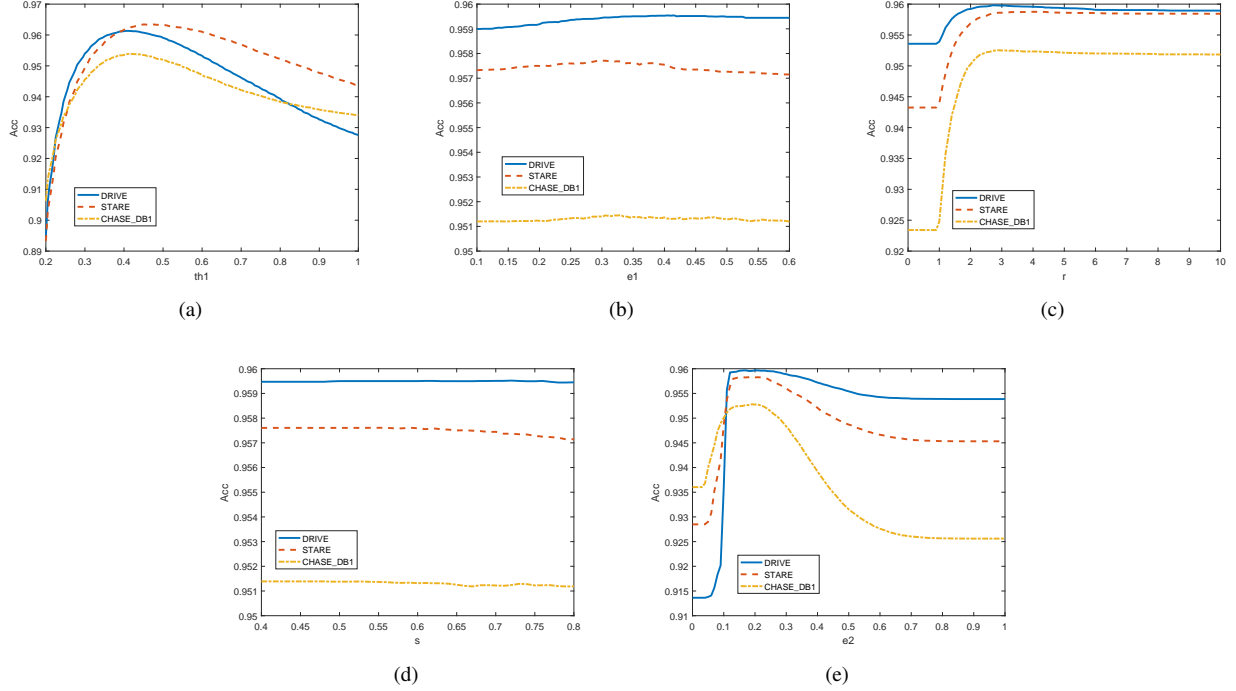


Fig. 10: The influence of different parameters. (a) Variations in mean segmentation accuracy by varying $th1$. (b) Variations in mean segmentation accuracy by varying $e1$. (c) Variations in mean segmentation accuracy by varying r . (d) Variations in mean segmentation accuracy by varying s . (e) Variations in mean segmentation accuracy by varying $e2$.

Y. In set X 12.7% pixels are marked as vessels while in set Y 12.3% are annotated as vessels.

STARE² [17] consists of 20 fundus images. These images are captured by a TopCon TRV-50 fundus camera at 35° FOV, and the size of each image is of 605×700 pixels. Ten images contain pathology while the other ten images are normal. The STARE dataset is annotated by two independent observers. The first observer (O_1) annotates 10.4% pixels as vessels while the second observer (O_2) segments 14.9% vessel pixels.

CHASE_DB1³ [28] consists of 28 fundus images acquired from multiethnic school children. These images are captured by a hand-held Nidek NM-200-D fundus camera at 30° FOV, and the size of each image is of 960×999 pixels. The CHASE_DB1 is annotated by two independent human observers, resulting in set $gt1$ and $gt2$.

B. Evaluation Metrics

In the process of retinal vessel segmentation, each pixel is classified as vessels or background, thereby resulting in four events: two correct classifications and two incorrect classifications, which are defined in Table IV.

TABLE IV: FOUR EVENTS OF VESSEL CLASSIFICATION

	Vessel present	vessel absent
vessel detected	True Positive (TP)	False Positive (FP)
vessel not detected	False Negative (FN)	True Negative(TN)

In order to evaluate the performance of the vessel segmentation algorithms, three commonly used metrics are applied.

$$\begin{aligned}
 \text{Sensitivity} &= \frac{TP}{TP + FN} \\
 \text{Specificity} &= \frac{TN}{TN + FP} \\
 \text{Accuracy} &= \frac{TP + TN}{TP + TN + FP + FN}
 \end{aligned}$$

Sensitivity (Se) reflects the algorithm's ability of detecting vessel pixels while Specificity (Sp) is a measure of the algorithm's effectiveness in identifying background pixels. Accuracy (Acc) is a global measure of classification performance combining both Se and Sp . The performance of the vessel segmentation method is also measured by the area under a receiver operating characteristic (ROC) curve (AUC). The conventional AUC is calculated from a number of operating points, and normally used to evaluate the balanced data classification problem. However, in practice the researchers need to select an operating point to compare their method with other methods. Also blood vessel segmentation is an unbalanced data classification problem, in which there are much fewer vessel pixels than the background pixels. In order to evaluate the performance of blood vessel segmentation properly, $AUC = (Se + Sp)/2$ [23], [37] is applied to indicate the overall performance of blood vessel segmentation, which is suitable to describe the overall performance of imbalanced data classification problem and specifically for the case when only one operating point is used. The segmentation time required per image in seconds for implementing the proposed

²<http://www.ces.clemson.edu/~ahoover/stare/>

³<https://blogs.kingston.ac.uk/retinal/chasedb1/>

segmentation algorithm in MATLAB on a Laptop with Intel Core i7 processor, 2.5GHz and 8GB RAM is recorded.

IV. EXPERIMENTS AND RESULTS

In this section, three sets of experiments are performed with the purpose of evaluating the proposed vessel segmentation algorithm. In the first experiment, parameters setting was provided. In the second experiment, vessel skeleton extraction was analyzed for segmentation performance. In the third experiment, the proposed method was compared with other supervised and unsupervised methods.

A. Parameters Setting

All parameters of the proposed algorithm are set as follows: $th1 = 0.35$, $e_1 = 0.35$, $r = 2.2$, $s = 0.53$, $e_2 = 0.25$. In order to demonstrate the sensitivity of the algorithm to these parameters, the variations in Acc by varying $th1$, e_1 , r , s and e_2 are given in Fig.10.(a), (b), (c), (d) and (e).

From Fig.10, it can be observed that the proposed algorithm can maintain high segmentation accuracy on the DRIVE, STARE and CHASE_DB1 datasets as $th1$ varies in $[0.3, 0.5]$ or e_2 varies in $[0.15, 0.3]$; For the parameters e_1 and s , the images from three datasets can maintain high segmentation accuracy when e_1 belongs to $[0.2, 0.4]$ or s belongs to $[0.4, 0.6]$; For the parameter r , the proposed method can achieve a high segmentation accuracy as s varies in $[2, 6]$. From the above observation, it can be seen that the algorithm is not sensitive to parameters when the parameters change in a relatively large range.

B. The Segmentation Performance and Analysis of Vessel Skeleton Extraction

The segmentation performance of the proposed algorithm on three public available datasets is given in Table V. From Table V, it can be observed that the proposed algorithm can achieve more than 95% segmentation accuracy on the DRIVE, STARE and CHASE_DB1 datasets, with the highest accuracy score is achieved in the DRIVE dataset. The exemplary segmentation results are shown in Fig.11.

Moreover, from Table V, it can be observed that vessel skeleton extraction can improve the performance of the proposed algorithm, especially the ability of detecting vessel pixels. With vessel skeleton extraction, the proposed method can achieve more than 5% increase of *Sensitivity* and 2% increase of *AUC*. Also the processing time is reduced when vessel skeleton extraction is applied.

C. Comparison With the Other Methods

Since most of researchers compare their algorithm with other methods by using manual segmentations from set X in the DRIVE dataset and the manual segmentations from the first observer in the STARE dataset, in our work the segmentations of set X are used as the ground truth for the DRIVE dataset, and for the STARE dataset, the segmentations of the first observer are used as the ground truth.

The segmentation performance and computational complexity of the proposed algorithm in comparison with other state-of-art methods on the DRIVE and STARE datasets are given in Table VI. From Table VI, it can be observed that for the DRIVE dataset, the accuracy of the proposed model are the highest among all existing methods with $Acc = 0.960$, $Se = 0.736$ and $Sp = 0.981$. On the STARE dataset, the accuracy and *AUC* of the proposed model are the highest among unsupervised methods with $Acc = 0.957$, $AUC = 0.880$. Although the supervised method [15] has the best performance on STARE dataset, the method is computationally more complex due to the use of deep neural networks, and the deep neural network may need retraining for new datasets. In addition, the proposed algorithm has a lower computational complexity than many other segmentation methods.

V. CONCLUSION AND DISCUSSION

In this paper, a novel unsupervised segmentation algorithm is proposed to extract blood vessels from the fundus images. The proposed method is inspired by image matting [24]–[26]. Image matting is a complicated and challenging problem, which aims to accurately extract a foreground from an image. Most image matting models are based on a user-specified trimap, which consists of foreground regions, background regions and undetermined regions. In essence, matting models make use of the priori knowledge (foreground knowledge and background knowledge) to estimate the undetermined regions, which can not be classified easily. Similarly, in a fundus image, a few vessel regions and background regions can be extracted easily without complicated extraction methods. Thus, the useful information from vessel regions and background regions can be applied to classify the pixels in the undetermined regions, which are difficult to be classified correctly. This is the basic idea of the proposed method. It is worthwhile to point out that by dividing the fundus image into vessel regions, background regions and undetermined regions, the computational complexity is decreased since the number of pixels which need to be further divided by classifier is reduced.

The proposed algorithm divides the enhanced vessel image into preliminary vessel regions, background regions and undetermined regions. Then a list of region features are defined and used to perform noise region removal. Also these region features are applied to extract the skeletons of blood vessels in fundus images. The region features characterize the morphological properties of blood vessels and are suitable for vessel segmentation. In order to classify the pixels in undetermined regions, HGA is proposed to label the undetermined pixels as vessel or non-vessel. HGA is inspired by the non-dominated sorting method, which is first by proposed by Deb *et.al* [34] and can effectively separate the overall non-dominated set of solutions into different ranks. HGA separates the undetermined pixels into different hierarchies according to the distance between the undetermined pixel and the closest vessel pixel, and then updates the undetermined pixels in an incremental way according to correlation functions.

The proposed algorithm is very efficient and effective in blood vessel segmentation, which achieves a segmentation

TABLE V: THE SEGMENTATION PERFORMANCE OF THE PROPOSED ALGORITHM ON THREE TEST DATASETS

Dataset	Ground-Truth	The Algorithm with Vessel Skeleton Extraction					The Algorithm without Vessel Skeleton Extraction				
		Acc	AUC	Se	Sp	Time(s)	Acc	AUC	Se	Sp	Time(s)
DRIVE Test	Set X	0.960	0.859	0.736	0.981	10.720	0.960	0.837	0.688	0.986	11.959
	Set Y	0.964	0.877	0.772	0.982		0.964	0.853	0.720	0.987	
STARE	O1	0.957	0.881	0.791	0.970	15.740	0.959	0.862	0.748	0.976	16.563
	O2	0.946	0.815	0.648	0.981		0.945	0.795	0.604	0.986	
CHASE_DB1	gt1	0.951	0.815	0.657	0.973	50.710	0.954	0.789	0.597	0.981	60.847
	gt2	0.950	0.812	0.652	0.971		0.952	0.783	0.588	0.978	

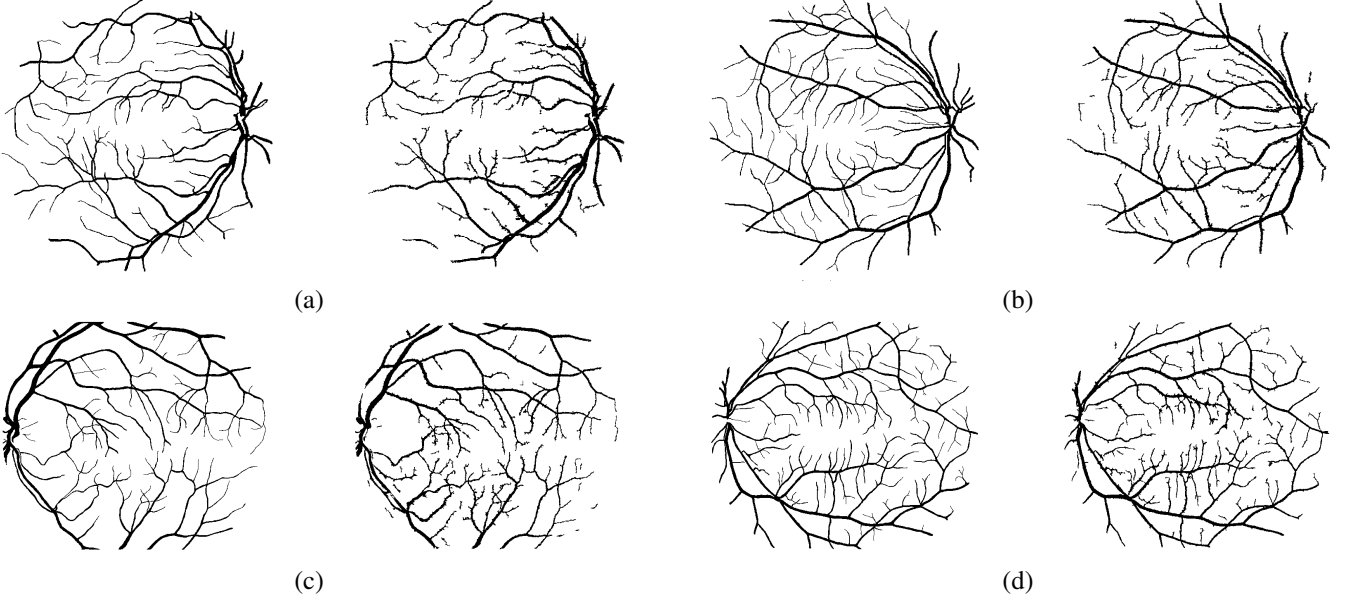


Fig. 11: Ground truth (left) and segmentation result (right): (a) and (b) are the images from DRIVE dataset, (c) and (d) are the images from the STARE dataset

TABLE VI: PERFORMANCE OF DIFFERENT SEGMENTATION MODELS ON THE DRIVE TEST AND STARE DATASETS

Test Datasets	DRIVE Test					STARE					
Methods	Acc	AUC	Se	Sp	Time	Acc	AUC	Se	Sp	Time	System
Supervised Methods											
Staal <i>et.al</i> [10]	0.944	-	-	-	15min	0.952	-	-	-	15min	1.0 GHz, 1-GB RAM
Soares <i>et.al</i> [11]	0.946	-	-	-	~3min	0.948	-	-	-	~3min	2.17 GHz, 1-GB RAM
Lupascu <i>et.al</i> [12]	0.959	-	0.720	-	-	-	-	-	-	-	-
Marin <i>et.al</i> [13]	0.945	0.843	0.706	0.980	~90s	0.952	0.838	0.694	0.982	~90s	2.13 GHz, 2-GB RAM
Roychowdhury <i>et.al</i> [14]	0.952	0.844	0.725	0.962	3.11s	0.951	0.873	0.772	0.973	6.7s	2.6 GHz, 2-GB RAM
Liskowski <i>et.al</i> [15]	0.954	0.881	0.781	0.981	-	0.973	0.921	0.855	0.986	-	NVIDIA GTX Tian GPU
Unsupervised Methods											
Hoover <i>et.al</i> [17]	-	-	-	-	-	0.928	0.730	0.650	0.810	5min	Sun SPARCstation 20
Mendonca <i>et.al</i> [19]	0.945	0.855	0.734	0.976	2.5min	0.944	0.836	0.699	0.973	3min	3.2 GHz, 980-MB RAM
Lam <i>et.al</i> [38]	-	-	-	-	-	0.947	-	-	-	8min	1.83 GHz, 2-GB RAM
Al-Diri <i>et.al</i> [21]	-	-	0.728	0.955	11min	-	-	0.752	0.968	-	1.2 GHz
Lam and Yan <i>et.al</i> [22]	0.947	-	-	-	13min	0.957	-	-	-	13min	1.83 GHz, 2-GB RAM
Perez <i>et.al</i> [39]	0.925	0.806	0.644	0.967	~2min	0.926	0.857	0.769	0.944	~2min	Parallel Cluster
Miri <i>et.al</i> [40]	0.943	0.846	0.715	0.976	~50s	-	-	-	-	-	3 GHz, 1-GB RAM
Budai <i>et.al</i> [41]	0.957	0.816	0.644	0.987	-	0.938	0.781	0.580	0.982	-	2.3 GHz, 4-GB RAM
Nguyen <i>et.al</i> [42]	0.941	-	-	-	2.5s	0.932	-	-	-	2.5s	2.4 GHz, 2-GB RAM
Yitian <i>et.al</i> [23]	0.954	0.862	0.742	0.982	-	0.956	0.874	0.780	0.978	-	3.1GHz, 8-GB RAM
Proposed	0.960	0.858	0.736	0.981	10.72s	0.957	0.880	0.791	0.970	15.74s	2.5 GHz, 4-GB RAM

accuracy of 96.0%, 95.7% and 95.1% on three public available datasets with an average time of 10.72s, 15.74s and 50.71s, respectively. The experimental results show that it has a low computational time and outperforms many other segmentation approaches. Redesigning the proposed algorithm for blood vessel segmentation on wide-field fundus images with greater than 200° FOV is a topic worth for further study.

REFERENCES

- [1] J. J. Kanski and B. Bowling, *Clinical Ophthalmology: A Systematic Approach*. Elsevier Health Sciences, 2011.
- [2] F. Zana and J.-C. Klein, "A multimodal registration algorithm of eye fundus images using vessels detection and hough transform," *IEEE Transactions on Medical Imaging*, vol. 18, no. 5, pp. 419–428, 1999.
- [3] M. Foracchia, E. Grisan, and A. Ruggeri, "Extraction and quantitative description of vessel features in hypertensive retinopathy fundus images," in *Book Abstracts 2nd International Workshop on Computer Assisted Fundus Image Analysis*, vol. 6, 2001.
- [4] C. Heneghan, J. Flynn, M. O'Keefe, and M. Cahill, "Characterization of changes in blood vessel width and tortuosity in retinopathy of prematurity using image analysis," *Medical Image Analysis*, vol. 6, no. 4, pp. 407–429, 2002.
- [5] E. Grisan and A. Ruggeri, "A divide et impera strategy for automatic classification of retinal vessels into arteries and veins," in *Engineering in Medicine and Biology Society, 2003. Proceedings of The 25th Annual International Conference of The IEEE*, vol. 1, 2003, pp. 890–893.
- [6] K. Fritzsche, A. Can, H. Shen, C. Tsai, J. Turner, H. Tanenbaum, C. Stewart, B. Roysam, J. Suri, and S. Laxminarayan, "Automated model based segmentation, tracing and analysis of retinal vasculature from digital fundus images," *State-of-The-Art Angiography, Applications and Plaque Imaging Using MR, CT, Ultrasound and X-rays*, pp. 225–298, 2003.
- [7] C. Mariño, M. G. Penedo, M. Penas, M. J. Carreira, and F. Gonzalez, "Personal authentication using digital retinal images," *Pattern Analysis and Applications*, vol. 9, no. 1, pp. 21–33, 2006.
- [8] A. Haddouche, M. Adel, M. Rasigni, J. Conrath, and S. Bourennane, "Detection of the foveal avascular zone on retinal angiograms using markov random fields," *Digital Signal Processing*, vol. 20, no. 1, pp. 149–154, 2010.
- [9] M. M. Fraz, P. Remagnino, A. Hoppe, B. Uyyanonvara, A. R. Rudnicka, C. G. Owen, and S. A. Barman, "Blood vessel segmentation methodologies in retinal images—a survey," *Computer Methods and Programs In Biomedicine*, vol. 108, no. 1, pp. 407–433, 2012.
- [10] J. Staal, M. D. Abramoff, M. Niemeijer, M. A. Viergever, and B. van Ginneken, "Ridge-based vessel segmentation in color images of the retina," *IEEE Transactions on Medical Imaging*, vol. 23, no. 4, pp. 501–509, 2004.
- [11] J. V. Soares, J. J. Leandro, R. M. Cesar, H. F. Jelinek, and M. J. Cree, "Retinal vessel segmentation using the 2-d gabor wavelet and supervised classification," *IEEE Transactions on Medical Imaging*, vol. 25, no. 9, pp. 1214–1222, 2006.
- [12] C. A. Lupascu, D. Tegolo, and E. Trucco, "Fabc: Retinal vessel segmentation using adaboost," *IEEE Transactions on Information Technology in Biomedicine*, vol. 14, no. 5, pp. 1267–1274, 2010.
- [13] D. Marín, A. Aquino, M. E. Gegúndez-Arias, and J. M. Bravo, "A new supervised method for blood vessel segmentation in retinal images by using gray-level and moment invariants-based features," *IEEE Transactions on Medical Imaging*, vol. 30, no. 1, pp. 146–158, 2011.
- [14] S. Roychowdhury, D. D. Koozekanani, and K. K. Parhi, "Blood vessel segmentation of fundus images by major vessel extraction and subimage classification," *IEEE Journal of Biomedical and Health Informatics*, vol. 19, no. 3, pp. 1118–1128, 2015.
- [15] P. Liskowski and K. Krawiec, "Segmenting retinal blood vessels with deep neural networks," *IEEE Transactions on Medical Imaging*, vol. 35, pp. 1–1, 2016.
- [16] A. F. Frangi, W. J. Niessen, K. L. Vincken, and M. A. Viergever, "Multiscale vessel enhancement filtering," in *International Conference on Medical Image Computing and Computer-Assisted Intervention*. Springer, 1998, pp. 130–137.
- [17] A. Hoover, V. Kouznetsova, and M. Goldbaum, "Locating blood vessels in retinal images by piecewise threshold probing of a matched filter response," *IEEE Transactions on Medical Imaging*, vol. 19, no. 3, pp. 203–210, 2000.
- [18] F. K. Quek and C. Kirbas, "Vessel extraction in medical images by wave-propagation and traceback," *IEEE Transactions on Medical Imaging*, vol. 20, no. 2, pp. 117–131, 2001.
- [19] A. M. Mendonca and A. Campilho, "Segmentation of retinal blood vessels by combining the detection of centerlines and morphological reconstruction," *IEEE Transactions on Medical Imaging*, vol. 25, no. 9, pp. 1200–1213, 2006.
- [20] K. Sum and P. Y. Cheung, "Vessel extraction under non-uniform illumination: A level set approach," *IEEE Transactions on Biomedical Engineering*, vol. 55, no. 1, pp. 358–360, 2008.
- [21] B. Al-Diri, A. Hunter, and D. Steel, "An active contour model for segmenting and measuring retinal vessels," *IEEE Transactions on Medical Imaging*, vol. 28, no. 9, pp. 1488–1497, 2009.
- [22] B. S. Lam, Y. Gao, and A. W.-C. Liew, "General retinal vessel segmentation using regularization-based multicavity modeling," *IEEE Transactions on Medical Imaging*, vol. 29, no. 7, pp. 1369–1381, 2010.
- [23] Y. Zhao, L. Rada, K. Chen, S. P. Harding, and Y. Zheng, "Automated vessel segmentation using infinite perimeter active contour model with hybrid region information with application to retinal images," *IEEE Transactions on Medical Imaging*, vol. 34, no. 9, pp. 1797–1807, 2015.
- [24] J. Wang and M. F. Cohen, "An iterative optimization approach for unified image segmentation and matting," in *Tenth IEEE International Conference on Computer Vision (ICCV'05) Volume 1*, vol. 2. IEEE, 2005, pp. 936–943.
- [25] K. He, C. Rhemann, C. Rother, X. Tang, and J. Sun, "A global sampling method for alpha matting," in *Computer Vision and Pattern Recognition (CVPR), 2011 IEEE Conference on*. IEEE, 2011, pp. 2049–2056.
- [26] Q. Chen, D. Li, and C.-K. Tang, "Knn matting," *IEEE Transactions on Pattern Analysis and Machine Intelligence*, vol. 35, no. 9, pp. 2175–2188, 2013.
- [27] P. Bankhead, C. N. Scholfield, J. G. McGeown, and T. M. Curtis, "Fast retinal vessel detection and measurement using wavelets and edge location refinement," *PloS One*, vol. 7, no. 3, p. e32435, 2012.
- [28] M. M. Fraz, P. Remagnino, A. Hoppe, B. Uyyanonvara, A. R. Rudnicka, C. G. Owen, and S. A. Barman, "An ensemble classification-based approach applied to retinal blood vessel segmentation," *IEEE Transactions on Biomedical Engineering*, vol. 59, no. 9, pp. 2538–2548, 2012.
- [29] T. Walter, P. Massin, A. Erginay, R. Ordonez, C. Jeulin, and J.-C. Klein, "Automatic detection of microaneurysms in color fundus images," *Medical Image Analysis*, vol. 11, no. 6, pp. 555–566, 2007.
- [30] E. Rakun, M. Andriani, I. W. Wiprayoga, K. Danniswara, and A. Tjandra, "Combining depth image and skeleton data from kinect for recognizing words in the sign system for indonesian language (sibi [sistem isyarat bahasa indonesia])," in *Advanced Computer Science and Information Systems (ICACSIS), 2013 International Conference on*. IEEE, 2013, pp. 387–392.
- [31] A. F. Banwell, M. Caballero, N. S. Arnold, N. F. Glasser, L. M. Cathles, and D. R. MacAyeal, "Supraglacial lakes on the larsen b ice shelf, antarctica, and at paakitsoq, west greenland: A comparative study," *Annals of Glaciology*, vol. 55, no. 66, pp. 1–8, 2014.
- [32] S. Roychowdhury, D. D. Koozekanani, and K. K. Parhi, "Iterative vessel segmentation of fundus images," *IEEE Transactions on Biomedical Engineering*, vol. 62, no. 7, pp. 1738–1749, 2015.
- [33] L. Lam, S.-W. Lee, and C. Y. Suen, "Thinning methodologies—a comprehensive survey," *IEEE Transactions on Pattern Analysis and Machine Intelligence*, vol. 14, no. 9, pp. 869–885, 1992.
- [34] K. Deb, A. Pratap, S. Agarwal, and T. Meyarivan, "A fast and elitist multiobjective genetic algorithm: Nsga-ii," *IEEE Transactions on Evolutionary Computation*, vol. 6, no. 2, pp. 182–197, 2002.
- [35] K. Deb and H. Jain, "An evolutionary many-objective optimization algorithm using reference-point-based nondominated sorting approach, part i: Solving problems with box constraints," *IEEE Transaction on Evolutionary Computation*, vol. 18, no. 4, pp. 577–601, 2014.
- [36] H. Li and Q. Zhang, "Multiobjective optimization problems with complicated pareto sets, moea/d and nsga-ii," *IEEE Transactions on Evolutionary Computation*, vol. 13, no. 2, pp. 284–302, 2009.
- [37] X. Hong, S. Chen, and C. J. Harris, "A kernel-based two-class classifier for imbalanced data sets," *IEEE Transactions on Neural Networks*, vol. 18, no. 1, pp. 28–41, 2007.
- [38] B. S. Y. Lam and H. Yan, "A novel vessel segmentation algorithm for pathological retina images based on the divergence of vector fields," *IEEE Transactions on Medical Imaging*, vol. 27, no. 2, pp. 237–246, 2008.
- [39] M. A. Palomera-Pérez, M. E. Martínez-Pérez, H. Benítez-Pérez, and J. L. Ortega-Arjona, "Parallel multiscale feature extraction and region growing: Application in retinal blood vessel detection," *IEEE Transactions*

- on Information Technology in Biomedicine*, vol. 14, no. 2, pp. 500–506, 2010.
- [40] M. S. Miri and A. Mahloojifar, “Retinal image analysis using curvelet transform and multistructure elements morphology by reconstruction,” *IEEE Transactions on Biomedical Engineering*, vol. 58, no. 5, pp. 1183–1192, 2011.
 - [41] I. Section, “Robust vessel segmentation in fundus images,” *International Journal of Biomedical Imaging*, vol. 2013, no. 6, p. 154860, 2013.
 - [42] U. T. Nguyen, A. Bhuiyan, L. A. Park, and K. Ramamohanarao, “An effective retinal blood vessel segmentation method using multi-scale line detection,” *Pattern Recognition*, vol. 46, no. 3, pp. 703–715, 2013.